JGR Space Physics

RESEARCH ARTICLE
10.1029/2023JA031578

Key Points:

- We evaluate the role of whistler-mode waves on relativistic electron precipitation by modeling ELFIN case-studies and statistics
- Observed precipitation >200 keV exceeds results obtained with empirical models of latitudinal wave power distributions, notably at night
- The discrepancy may be explained by mid-to-high-latitude intense whistler-mode waves which are missing from current empirical models

Correspondence to:
E. Tsai,
ethantsai@ucla.edu

Citation:
Tsai, E., Artemyev, A., Angelopoulos, V., & Zhang, X.-J. (2023). Investigating whistler-mode wave intensity along field lines using electron precipitation measurements. *Journal of Geophysical Research: Space Physics*, *128*, e2023JA031578. https://doi.org/10.1029/2023JA031578

Received 11 APR 2023
Accepted 21 JUL 2023

Author Contributions:
Conceptualization: Ethan Tsai, Anton Artemyev
Data curation: Anton Artemyev, Xiao-Jia Zhang
Formal analysis: Ethan Tsai, Anton Artemyev
Funding acquisition: Anton Artemyev, Vassilis Angelopoulos, Xiao-Jia Zhang
Investigation: Ethan Tsai, Anton Artemyev
Methodology: Ethan Tsai, Anton Artemyev
Project Administration: Vassilis Angelopoulos
Software: Ethan Tsai
Supervision: Vassilis Angelopoulos
Validation: Ethan Tsai, Anton Artemyev, Xiao-Jia Zhang
Writing – original draft: Ethan Tsai, Anton Artemyev
Writing – review & editing: Ethan Tsai, Anton Artemyev, Vassilis Angelopoulos, Xiao-Jia Zhang

Investigating Whistler-Mode Wave Intensity Along Field Lines Using Electron Precipitation Measurements

Ethan Tsai[1], Anton Artemyev[1,2], Vassilis Angelopoulos[1], and Xiao-Jia Zhang[1,3]

[1]Earth, Planetary, and Space Sciences, University of California, Los Angeles, Los Angeles, CA, USA, [2]Space Research Institute of Russian Academy of Sciences, Moscow, Russia, [3]Department of Physics, The University of Texas at Dallas, Richardson, TX, USA

Abstract Electron fluxes in Earth's radiation belts are significantly affected by their resonant interaction with whistler-mode waves. This wave-particle interaction often occurs via first cyclotron resonance and, when intense and nonlinear, can accelerate subrelativistic electrons to relativistic energies while also scattering them into the atmospheric loss cone. Here, we model Electron Losses and Fields INvestgation's (ELFIN) low-altitude satellite measurements of precipitating electron spectra with a wave-electron interaction model to infer the profiles of whistler-mode intensity along magnetic latitude assuming realistic waveforms and statistical models of plasma density. We then compare these profiles with a wave power spatial distribution along field lines from an empirical model. We find that this empirical model is consistent with observations of subrelativistic (<200 keV) electron precipitation events, but deviates significantly for relativistic (>200 keV) electron precipitation events at all *MLT*s, especially on the nightside. This may be due to the sparse coverage of wave measurements at mid-to-high latitudes which causes statistically averaged wave power to be likely underestimated in current empirical wave models. As a result, this discrepancy suggests that intense waves likely do propagate to higher latitudes, although further investigation is required to quantify how well this high-latitude population can account for the observed relativistic electron precipitation.

Plain Language Summary Whistler-mode waves, the most prevalent type of plasma wave in Earth's magnetosphere, often interact with electrons by resonating with them, causing them to be accelerated and lost into Earth's atmosphere (in other words, precipitated). These waves are generated at the equator and typically stay constrained to within 20° in latitude; however, they can sometimes propagate to greater than 30° where they can accelerate electrons to relativistic energies. It is difficult to quantify how large of a contribution these mid-to-high-latitude waves have on radiation belt electrons due to a lack of off-equatorial spacecraft wave measurements. However, previous studies have shown that the energy spectra of precipitating electron fluxes may be used to infer the latitudinal extent of whistler-mode waves. We therefore compare measurements of relativistic precipitation from NASA's Electron Losses and Fields INvestgation (ELFIN) mission (a pair of CubeSats built and operated by UCLA) with large ensemble test-particle simulations informed by current empirical models of waves. Discrepancies in this comparison suggest that this elusive population of mid-to-high-latitude whistler-mode waves is most apparent at Earth's nightside and may even help explain some of the more intense precipitation events observed by the ELFIN CubeSats.

1. Introduction

Energetic electron fluxes in the Earth's radiation belts vary significantly in response to resonant electron interactions with whistler-mode waves (Shprits et al., 2008, and references therein). Such interactions can accelerate plasma sheet electrons to relativistic (e.g., Meredith et al., 2002; Millan & Baker, 2012; Thorne et al., 2013) or even ultrarelativistic (Allison & Shprits, 2020) energies, and pitch angle scatter energetic electrons into the loss cone causing their precipitation to the atmosphere (e.g., Millan & Thorne, 2007). This multifaceted role of whistler-mode waves makes them a key element of radiation belt dynamics (see discussion in Bortnik and Thorne (2007) and Thorne (2010)) and motivates investigation of whistler-mode wave characteristics and their relationship to electron precipitation (see Agapitov et al., 2013; Li et al., 2011; Meredith et al., 2001, 2012; Santolík et al., 2003; Wang et al., 2019). In addition to the importance of the wave frequency (which is typically fixed for very intense chorus mode waves, see Li et al., 2011; Tsurutani & Smith, 1974), there are two other defining wave characteristics: wave intensity (which determines electron scattering amplitudes, see reviews by Lyons and Williams (1984) and Schulz and Lanzerotti (1974)) and wave normal angle (which determines the resonance

energy range, see Albert, 2017; Artemyev et al., 2016; Lorentzen et al., 2001; Shprits & Ni, 2009), both of which vary with magnetic latitude (i.e., along magnetic field lines, or henceforth referred to simply as just latitude) (Agapitov et al., 2013, 2018; Santolík et al., 2014). The latitudinal profiles of these wave characteristics along field lines therefore define the relative efficiency of electron acceleration and scattering as a function of energy (e.g., Agapitov et al., 2018; Mourenas et al., 2012, 2014; Summers & Ni, 2008; Wang & Shprits, 2019). In particular, intense field-aligned whistler-mode waves can effectively resonate with relativistic electrons at mid-to-high latitudes since higher latitudes result in a monotonic increase of electron cyclotron-to-plasma frequency ratio, thereby increasing the minimum resonance energy (see, e.g., Summers et al., 2007; Thorne et al., 2005). Because intense relativistic electron precipitation is a fairly common observation (e.g., Artemyev et al., 2021; L. Chen et al., 2022; Grach et al., 2022; Mourenas, Artemyev, et al., 2022; Tsai et al., 2022), it is important to quantify the latitudinal extent of whistler-mode wave power that might enable such precipitation. This insight would help determine under what ambient wave propagation conditions and equatorial source properties mid-to-high-latitude wave propagation might take place.

Most intense whistler-mode waves are near-equatorial ($\lesssim$20° in latitude) and are typically found at the nightside injection region (Meredith et al., 2012). Their near-equatorial localization has been attributed to the increasing wave obliquity expected with propagation away from their equatorial source (Agapitov et al., 2013; Breuillard et al., 2012; L. Chen et al., 2013) and their severe damping by Landau resonance with suprathermal electrons (e.g., Bell et al., 2002; Bortnik et al., 2007). This effect is moderated at the dayside, where low intensity waves are observed at much higher latitudes than at the nightside (Meredith et al., 2012). This moderation is attributed to wave propagation in the presence of gentler gradients in the ambient dayside magnetic field (due to magnetospheric compression), and the lower density of suprathermal electrons (Li et al., 2010; Walsh et al., 2020)—both of which reduce wave damping. Reduced damping then allows whistler-mode waves on the dayside to propagate up to 30–40° (Agapitov et al., 2018). This day-night asymmetry in the propagation latitude of whistler-mode waves has been used to explain the preponderance of relativistic microburst precipitation (i.e., very intense short-lived precipitation events, see Blum et al., 2015; Breneman et al., 2017; Douma et al., 2019; O'Brien et al., 2004; Zhang, Angelopoulos, et al., 2022) in the dawn-noon sector (see discussion in Thorne et al. (2005)). However, an observational determination of the midlatitude wave intensity needed to explain the precipitating fluxes of relativistic electrons has not yet been undertaken. In the past, this has been in great part due the lack of availability of keV to MeV energy electron flux data with sufficient energy resolution and precipitating-to-trapped flux ratio fidelity. Several recent case studies of relativistic electron microbursts have examined precipitating electron fluxes and energy ranges (e.g., L. Chen et al., 2022; Miyoshi et al., 2020, 2021) using ducted wave propagation (when wave rays are trapped by local density perturbations that form a duct along field lines, see general theory in, e.g., Helliwell, 1965; Karpman & Kaufman, 1982; Pasmanik & Trakhtengerts, 2005; Streltsov & Bengtson, 2020), that is, excluding any damping and wave intensity decay away from the equatorial source region. Both ray tracing simulations and spacecraft observations have confirmed that even weak density perturbations can result in ducting (R. Chen et al., 2021; Hanzelka & Santolík, 2019, 2022; Hosseini et al., 2021; Shen et al., 2021; Yearby et al., 2011), while more effective ducting would allow waves to propagate so far that even ground-based VLF receivers can pick them up (e.g., Demekhov et al., 2017; Martinez-Calderon et al., 2016, 2020; Titova et al., 2017). However, statistical studies using ground-based observations (Douma et al., 2018; Martinez-Calderon et al., 2015; Simms et al., 2019) and mid-to-high-latitude spacecraft measurements have yet to yield an estimate of the occurrence rate of ducted waves due to their low occurrence rates and sparse coverage. As a result, the contribution of ducted waves to statistical wave power averages is likely smoothed out in current empirical models of whistler-mode waves (Agapitov et al., 2013; Meredith et al., 2012). Yet, it has been shown that even the infrequent presence of large amplitude, bursty, and likely ducted waves at midlatitudes could have an appreciable effect on radiation belt dynamics (Tsai et al., 2022). This study aims to use recently acquired, high energy and pitch angle resolution electron data from the ELFIN mission, to provide further insight into the contribution of high-latitude whistler waves to radiation belt electron losses.

We will compare directly measured precipitating electron spectra, as measured by the ELFIN CubeSats (Angelopoulos et al., 2020), to precipitation simulated in realistic plasma and magnetic field conditions, with typical whistler-mode waveforms and statistical models of wave power latitudinal and L shell distributions. This investigation is a natural continuation of several previous case studies demonstrating the potential importance of whistler-mode wave ducting utilizing ELFIN observations (Artemyev et al., 2021; L. Chen et al., 2022; Tsai et al., 2022). We judiciously select a number of precipitation events that span different *MLT* sectors and L shell

ranges to study with our simulation. Our test-particle simulations (Tsai et al., 2022) employ a synthetic empirical whistler-mode wave intensity model (Agapitov et al., 2018) detailed in Sections 2 and 3. We find that subrelativistic electron precipitation is in good agreement with expectation from our simulation when utilizing prior models of statistically averaged wave power latitudinal distributions. However, relativistic electron precipitation spectra, especially on the nightside, cannot be explained by whistler-mode wave-scattering of electrons from the same statistically averaged wave power latitudinal distributions. This mismatch therefore suggests that a transient population of mid-to-high-latitude whistler-mode waves must be present to enable bursty and energetic precipitation, but remain ephemeral enough so as to not increase the wave power averages in statistical models. We present our results for individual events in Section 4. Section 5 covers statistical results using our test-particle model and ELFIN observations with wide *MLT* coverage. In Section 6, we conclude with a summary of our results and possible approaches for inclusion of ducted whistler-mode wave population into radiation belt models.

2. Data Sets

The polar-orbiting ELFIN satellites provide precipitating fluxes from a low-altitude vantage point (Angelopoulos et al., 2020). Two identical CubeSats, ELFIN-A (ELA) and ELFIN-B (ELB), each equipped with an Energetic Particle Detector for Electrons (EPDE), measure pitch angle resolved fluxes from 50 keV to 5 MeV over 16 energy bins, while spinning at ∼21 revolutions per min. The energy resolution ($\Delta E/E < 40\%$) and angular resolution (16 sectors per spin, or ∼22.5° spin phase resolution), allows ELFIN to adequately resolve the bounce loss cone (which is much larger, ∼70° at ∼400 km). From this unique vantage point, ELFIN traverses the L shell ranges $3 < L < 18$ within ∼6 min 4 times per orbit. Each traversal, known as a "science zone crossing," provides a radial snapshot of equatorial processes at a given *MLT*.

Although the full statistical study uses ELFIN data up to June 2022, only 12 events were selected first as representative examples for case studies. They all feature a bursty precipitation event, classified as 1–7 contiguous spins (∼3 s < t < 21 s) with a strong ($j_{prec}/j_{trap} > 0.5$) precipitating-to-trapped flux ratio (hereafter, trapped refers to fluxes near-perpendicular to the magnetic field, i.e., locally trapped, but may be within the drift loss cone) while spanning all *MLT*s except for the dusk sector. Note that this relatively long precipitation observation that is on the order of seconds are typically attributed to either ELFIN's crossing of multiple whistler-mode equatorial source regions (see details regarding temporal/spatial variation of ELFIN-observed precipitation patterns in Zhang et al. (2023)) or to the natural spread of whistler-mode waves propagating along curved magnetic field lines (see Kang et al., 2022, for further discussion regarding the spatial spread of precipitation produced by a very localized equatorial whistler-mode source).

Table 1 itemizes these events and their properties. We took special care to exclude ambiguous events that had signatures of EMIC-wave driven precipitation (see examples of EMIC-driven precipitation events observed by ELFIN in Grach et al. (2022), An et al. (2022), Angelopoulos et al. (2022), and Capannolo et al. (2023)) or field-line scattering signatures (see, e.g., Artemyev, Angelopoulos, et al., 2022) not only in these 12 case studies, but also for the ∼6,000 orbits (∼8,500 science zones) used for the statistical portion of this study. In addition, we only included events where energy spectra was monotonically decreasing to reduce rare phenomena such as microbursts (see Zhang, Angelopoulos, et al., 2022, for more details regarding ELFIN observations of microbursts) that may skew results. All data were processed to exclude low counts/statistically insignificant data points (i.e., electronic noise).

We used three data products derived from ELFIN's EPDE data set: the energy spectrograms of trapped electron fluxes $j_{trap}(E)$ (outside the local bounce loss cone), the energy spectra of precipitating electron fluxes $j_{prec}(E)$ (moving toward the ionosphere within the local bounce loss cone), and the precipitating-to-trapped flux ratio j_{prec}/j_{trap}. Figure 1 shows two example events from our data set: the first two panels of 1a and 1b show the spectrograms of precipitating and trapped fluxes for each event, respectively, whereas the third panels show the spectrograms of the ratio of precipitating-to-trapped fluxes. The precipitation bursts marked by red and purple boxes are observed well inside the outer radiation belt, the region characterized by high intensity relativistic electron trapped fluxes (horizontal orange bar above panels). Sporadic peaks of the j_{prec}/j_{trap} ratio due to localized electron scattering by whistler-mode waves are seen at those times. The plasmasphere is also denoted (horizontal cyan line) and is defined as occurring immediately below the latitude where 300 keV trapped electron fluxes first fall below sensitivity level (presumably due to whistler-mode hiss waves; see further discussions regarding identifying different magnetospheric regions in ELFIN observations in Mourenas et al. (2021) and Angelopoulos et al. (2022)).

Table 1
Locations of and Geomagnetic Activity Conditions for the 12 Events Chosen for This Paper on the Basis of Exhibit Signatures of Nonlinear Wave-Particle Interaction

Figure	CubeSat	Precipitation timerange (UTC)	*MLT* sector	*L* shell	*MLT*	*Kp*	Match
Figure 2a	ELA	3 February 2021 20:46:37–20:46:50	Dawn/Day	6.2	5.8	3	✅
Figure 2b	ELA	3 February 2021 20:47:13-20:47:33	Dawn/Day	7.5	5.7	3	✅
Figures 1a and 2c	ELB	6 January 2021 11:53:50–11:54:01	Dawn/Day	7.1	8.4	2	✅
Figure 2d	ELA	1 October 2021 08:10:02–08:10:13	Dawn/Day	6.6	8.8	3	❌
Figure 2e	ELA	1 October 2021 04:59:57–05:01:18	Dawn/Day	6.4	10.2	4	✅
Figure 2f	ELA	1 November 2021 04:23:34–04:23:44	Dawn/Day	6.1	13.1	3	❓
Figure 3a	ELA	11 January 2021 17:50:50–17:50:58	Night	4.8	19.0	3	❓
Figure 3b	ELA	3 February 2021 13:42:25–13:42:32	Night	6.6	19.3	3	❓
Figure 3c	ELA	3 February 2021 09:01:43–09:01:56	Night	5.1	20.2	2	✅
Figure 3d	ELA	2 November 2021 22:18:21–22:18:35	Night	4.5	20.8	2	❌
Figure 3e	ELB	26 September 2020 01:01:12–01:01:20	Night	4.8	2.6	4	❌
Figures 1b and 3f	ELA	4 September 2020 01:12:24–01:12:33	Night	6.5	3.8	3	❌

Note. Half were chosen in dawn/day sector, while the other half were chosen in the night sector. Events were selected to have fairly uniform coverage in each sector. The "Match" column refers to how well the model agrees with ELFIN data which will be discussed further in Section 4 using Figures 2 and 3.

Figure 1c shows the primary derived data product used in our study: the energy spectrum of the j_{prec}/j_{trap} flux ratio averaged over the duration of the precipitation burst.

We next compare ELFIN's in situ flux ratios j_{prec}/j_{trap} with those from test-particle simulations in the presence of waves with amplitudes determined by an empirical chorus wave power distribution model. The wave amplitude model, which is based on a combination of 4 years of Van Allen Probe observations and 10 years of Cluster observations (Agapitov et al., 2018), provides the latitudinal distribution of whistler-mode wave intensity we use in our simulation (see Section 3).

3. Simulation of Wave-Particle Interactions

We build on our previous Julia-based (Bezanson et al., 2017; Rackauckas & Nie, 2017) test-particle simulation (Tsai et al., 2022), which utilizes the Hamiltonian formulation for wave-particle resonant interaction (Albert et al., 2013; Vainchtein et al., 2018), with some modifications to facilitate comparisons with case studies having limited equatorial information (Tsai, 2023). The equations of motion already incorporate nonlinear effects such as phase bunching, phase trapping, and anomalous trapping (Albert et al., 2021; Bortnik et al., 2008; Demekhov et al., 2006; Katoh et al., 2008; Kitahara & Katoh, 2019; Omura et al., 2007). The wave field includes the function $g(\phi)$—which describes the discretization of wave-packets as a function of wave phase (Mourenas, Zhang, et al., 2022; Zhang et al., 2020)—and the function $f(\lambda)$—which describes the wave amplitude variation along magnetic field lines. A key modification for this study is the implementation of an empirical chorus wave model $f(\lambda) \rightarrow B_w(\lambda, L, MLT, Kp)$ (see model and coefficients in Agapitov et al. (2018)) which allows us to compute with our test-particle simulations the expected precipitation rate consistent with statistically averaged wave intensity latitudinal profiles.

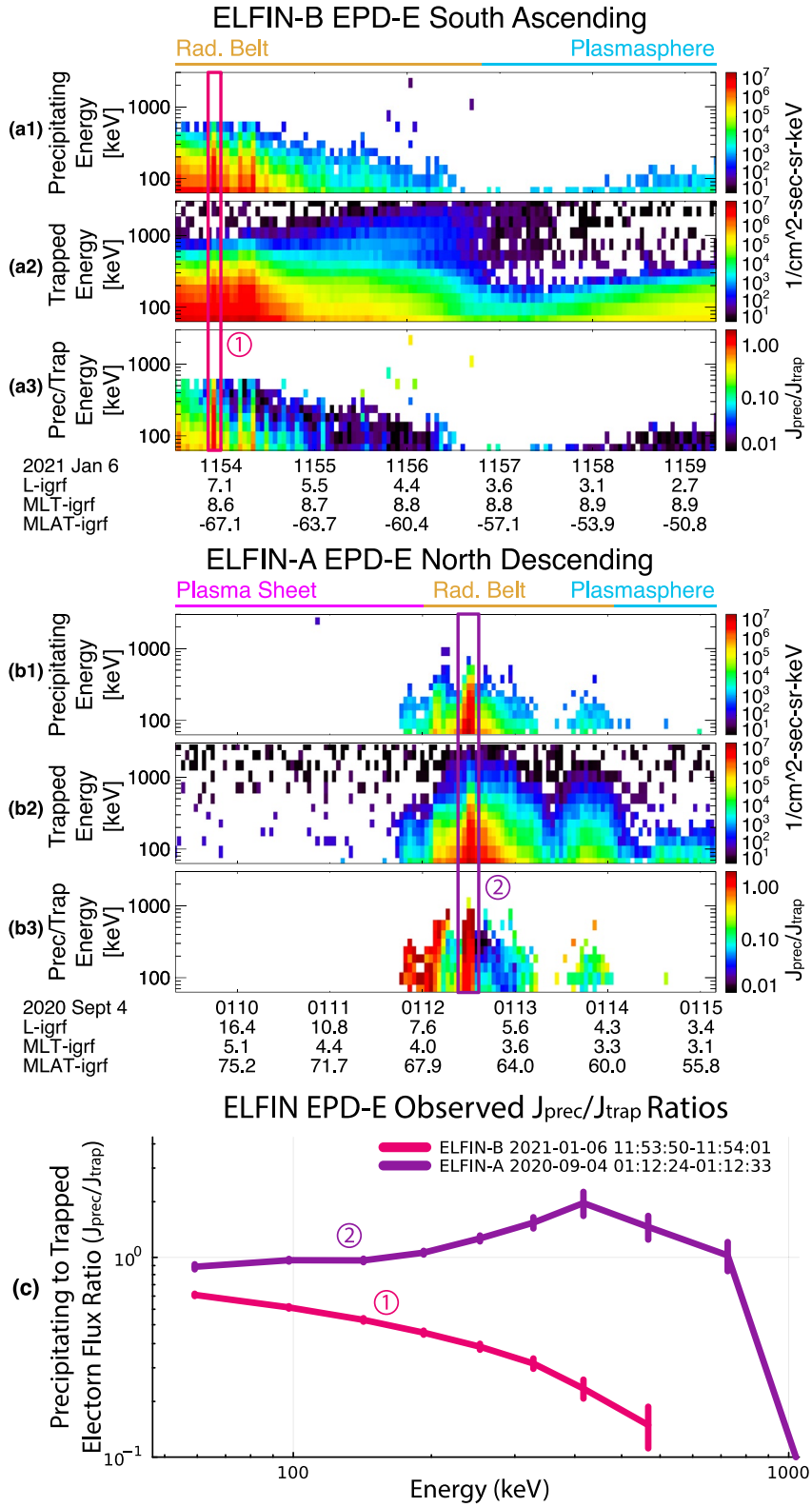

Figure 1. Panels (a) and (b) show Electron Losses and Fields INvestgation (ELFIN) observations of two science zone crossings. The three subpanels show, from top to bottom, energy spectra of precipitating fluxes, trapped fluxes, and precipitating-to-trapped flux ratios, respectively. Panel (c) shows the energy spectra of the precipitating-to-trapped electron flux ratios for their respective boxed time-ranges (1) and (2) during which short-lived but intense precipitation is observed.

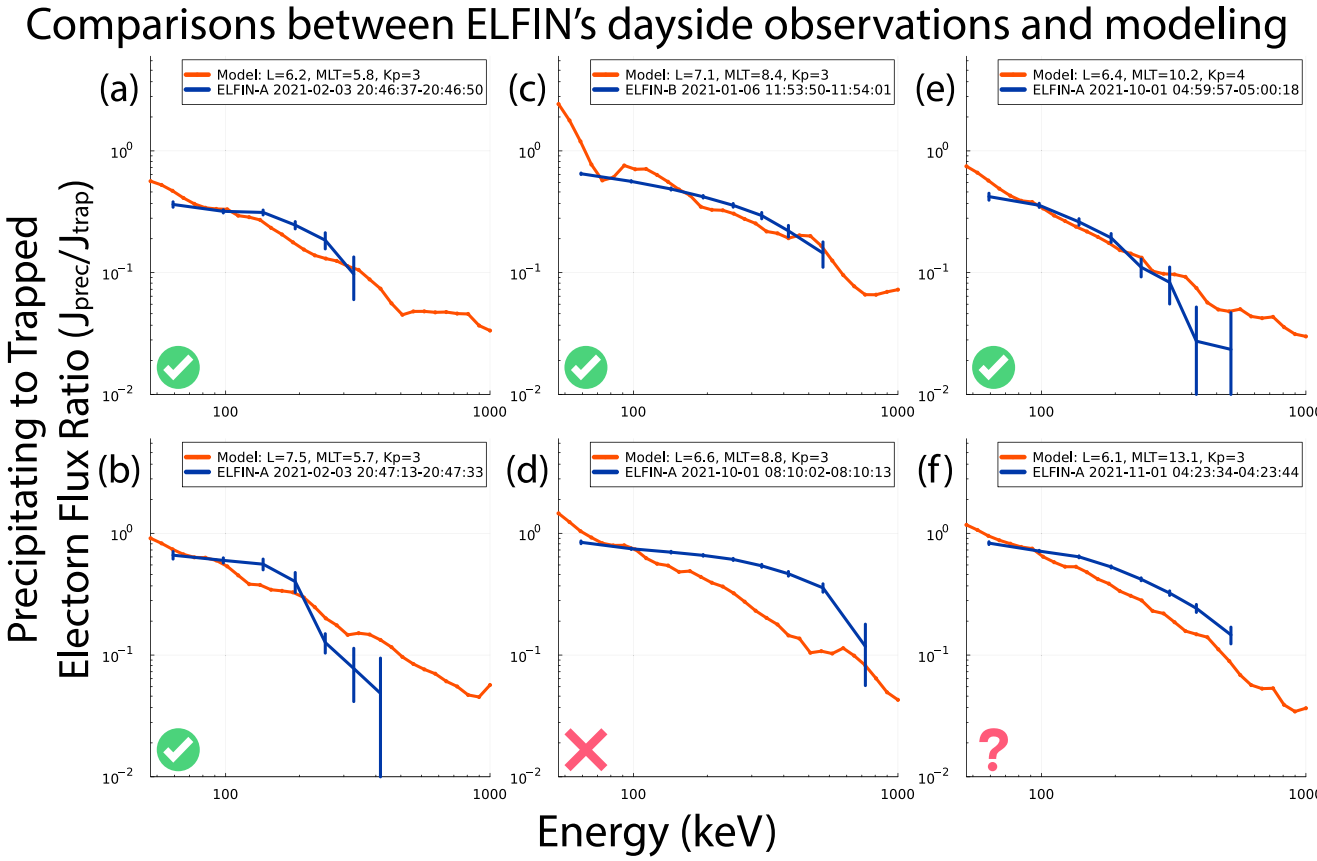

Figure 2. Comparisons between Electron Losses and Fields INvestgation (ELFIN) observations (dark blue) and modeling using empirical wave model (orange) on the dayside ($4 < MLT < 15$). The error bars on ELFIN data denote statistical variance. Checkmarks, question marks, and crosses denote good, questionable, and bad matches, respectively.

$$\log_{10}(B_w(\lambda, Kp, L, MLT)\,[\mathrm{nT}]) = b_0(\lambda - b_3)\cdot\exp(-\lambda b_2 - b_1) \tag{1}$$

$$f(\lambda) = C\cdot B_w\cdot\tanh(\lambda/1^\circ) \tag{2}$$

where coefficients b_i are provided by the empirical model as a function of L and MLT and λ is the latitude in degrees. C normalizes the wave amplitude function to a maximum at unity, while the $\tanh(\lambda/1^\circ)$ term describes wave growth out of the source region (Demekhov, 2011; Katoh & Omura, 2007; Tao et al., 2017). We further modify Agapitov et al. (2018) empirical model in two essential ways.

First, we change the MLT classification since the coefficients for $12 < MLT < 23$ are skewed by the relative lack of whistlers in the dusk flank range of $15 < MLT < 23$. As a result, we use $18 < MLT < 4$ instead of $23 < MLT < 4$ for nightside scenarios and $4 < MLT < 15$ instead of $4 < MLT < 12$ for dayside scenarios. Thus, the dusk flank is restricted to just $15 < MLT < 18$ and, at least for the case studies, we simply avoid choosing ELFIN observations from this MLT range.

Second, we set the minimum Kp in this model to 3, even if in reality the ELFIN measurements occur when $Kp < 3$. This is because strong, short-lived precipitation does not correlate well with Kp-index; it is instead more appropriately associated with AE activity tracing electron injections (see dependence of wave intensity on AE in Meredith et al. (2012), and references therein). As such, the presence of intense and bursty precipitation indicates locally active geomagnetic conditions that would be associated with $Kp = 3$ for test-particle simulation purposes, despite the reported value of Kp being <3. However, when the reported Kp is >3, then we opt to use that reported value in the simulation as well.

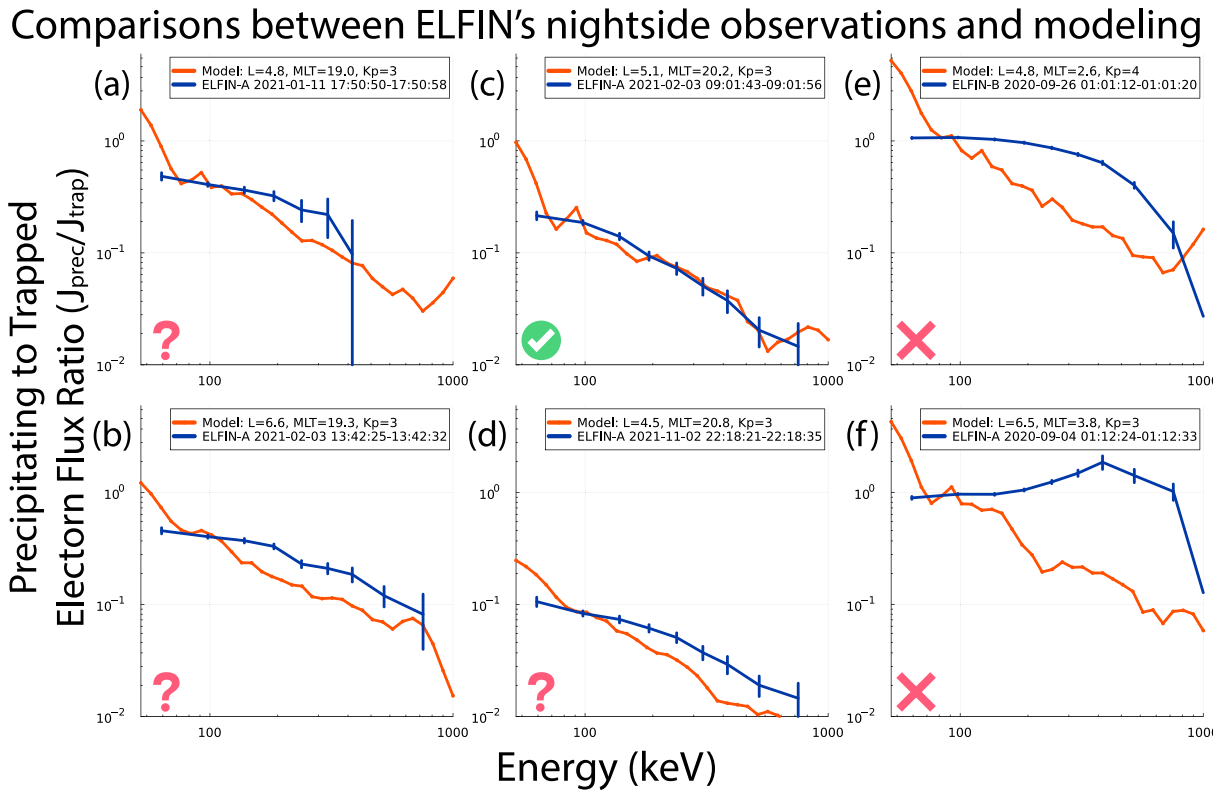

Figure 3. Comparisons between Electron Losses and Fields INvestgation (ELFIN) observations (dark blue) and modeling using empirical wave model (orange) on the nightside ($18 < MLT < 4$). The error bars on ELFIN data denote statistical variance. Checkmarks, question marks, and crosses denote good, questionable, and bad matches, respectively.

With the prescribed wave field now fully defined, we return to the equations of motion used in the test-particle simulation. These can be derived from the Hamiltonian as follows:

$$\dot{z} = \frac{p_z}{m_e\gamma}, \quad \dot{p}_z = -\frac{\mu B_0'}{\gamma} - \frac{eB_w f(z)}{\gamma}\sqrt{\frac{2\mu B_0}{m_e c^2}}\left(g(\phi)\cos\zeta + \frac{dg}{d\phi}\sin\zeta\right) \tag{3a}$$

$$\dot{\phi} = k\dot{z} - \omega, \quad \dot{\zeta} = k\dot{z} - \omega + \frac{eB_0}{m_e c\gamma} + \frac{e^2 B_w f(z)}{2\mu k m_e c\gamma}\sqrt{\frac{2\mu B_0}{m_e c^2}}(g(\phi)\sin\zeta) \tag{3b}$$

$$\dot{\mu} = -\frac{e^2 B_w f(z)}{k m_e c\gamma}\sqrt{\frac{2\mu B_0}{m_e c^2}}(g(\phi)\cos\zeta) \tag{3c}$$

where z, p_z are the field-aligned coordinate and momentum; $\zeta = \phi + \psi$ with gyrophase ψ and wave phase ϕ, which is determined by frequency ω and wave number $k(z, \omega)$ (Stix, 1962); μ is the magnetic moment; $' = \partial/\partial z$, $dg/d\phi$ is not neglected (important for small wave packet sizes); however, terms $\sim df/dz$ are neglected (for more details, refer to Section 3: Simulation Implementation in Tsai et al. (2022)). The electron trajectory is determined by energy $m_e c^2(\gamma - 1)$ where

$$\gamma = \sqrt{1 + \left(\frac{p_z}{m_e c}\right)^2 + \frac{2\mu B_0(z)}{m_e c^2}}$$

and equatorial pitch angle, α_{eq}, is given by $\sin(\alpha_{eq}) = 2\mu B_0(0)/(\gamma^2 - 1)$. The background magnetic field $B_0(z)$ is given by a curvature-free dipole model (Bell, 1984), and we relate the field-aligned coordinate z with magnetic latitude λ through the dipole equation: $dz = R_E L\sqrt{1 + 3\sin^2\lambda}\cos\lambda d\lambda$.

For each event, we perform a forward-modeling (as opposed to an inverse-modeling) procedure, where we obtain the latitudinal wave amplitude distribution based on the ELFIN's L, MLT, and Kp during the precipitation burst and then check whether the precipitation spectrum from our test-particle simulations is in agreement with the observations. In Figure 1a event, for example, the precipitation burst was observed by ELFIN-B on 6 January 2021 between 11:53:50 and 11:54:01 UTC. We use T89 (Tsyganenko, 1989) to map ELFIN-B's location at $L = 7.1$ and $MLT = 8.4$. For this event, $Kp = 2$ was obtained from the Kyoto/GFZ Potsdam database, but for modeling we use minimum $Kp = 3$. All three variables are then used to determine the coefficients used in Equation 1 (Agapitov et al., 2018). A test-particle simulation is then run using the following parameters:

1. An empirical model B_w for whistler-mode wave intensity, modified as described in Equation 2.
2. A plasma density model for equatorial plasma density (Sheeley et al., 2001).
3. An empirical model to account for plasma density variation along the field line as: $\omega_p/\omega_p(0) = \cos^{-5/2}\lambda$ (Denton et al., 2006).
4. A large ensemble consisting of $N = 2.5 \times 10^5$ particles spanning initial pitch angles $3° \le \alpha_0 \le 15°$ (we only care about electrons near the loss cone, which is set to 3°, further explained below).
5. Thirty-two energy bins from 50 keV to 1 MeV with 50× more particles in the highest energy bin compared to lowest to increase high energy precipitation statistics.

Particles are then simulated for just one bounce period, that is, particle tracing is terminated upon return to the equatorial plane, $z = 0$. This allows us to understand the scattering efficiency of a single interaction between the electron with the whistler-mode wave packet. Since wave occurrence, max amplitude, and equatorial electron phase space density are not known, we cannot use our simulation to predict absolute fluxes like we did in previous work (see Tsai et al., 2022). Rather, we are interested in determining and comparing the relative fluxes of precipitating electrons especially at higher energies where we expect the differences between our simulations and observations to be greatest.

In order to obtain the simulated precipitating-to-trapped electron flux ratio, we first set the equatorial loss cone to $\alpha_{LC} = 3°$. At ELFIN's altitude, the locally mirroring electrons map to around twice α_{LC}, so we consider simulated electrons with $\alpha_{final} < 3°$ as precipitating (j_{prec}) and those $3° < \alpha_{final} < 6°$ as trapped (j_{trap}). In a single interaction, electrons cannot lose more than a couple degrees in pitch angle, so we limit the upper bound of our simulation to 15° to save on simulation time. Finally, j_{prec}/j_{trap} can easily be computed for each of the 32 energy bins and directly compared to ELFIN's 16 energy bins.

4. Precipitation Events

Figures 2 and 3 show comparisons between j_{prec}/j_{trap} derived from test-particle simulations and ELFIN-observed j_{prec}/j_{trap} during the precipitation bursts of all 12 case studies. Both of these figures are meant to demonstrate the viability of the comparisons; as such, the conclusions drawn in this section serve only to qualitatively foreshadow the statistical results in Section 5. Additionally, note that simulated j_{prec}/j_{trap} is normalized to the mean of ELFIN's first two energy bins (j_{prec}/j_{trap}(~80 keV)): this is functionally equivalent to setting the equatorial wave amplitude consistent with ELFIN observations of electron precipitation (the ~30−100 keV precipitating-to-trapped electron flux ratio has been known to correlate well with the equatorial wave amplitude, see Li et al., 2013; Ni et al., 2014). As mentioned earlier, the primary quantity to compare between our simulation output and data is the relative energy profile (not the absolute value) of j_{prec}/j_{trap}. We use three important properties of radiation belt electron scattering to justify this comparison: (a) electrons can be diffusively scattered even by monochromatic waves due to the strong background (dipole) magnetic field gradient (Albert, 2001, 2010; Shklyar, 2021), (b) for monochromatic waves, each latitude corresponds to a specific resonance energy for fixed equatorial pitch angle (equal to the loss cone pitch angle), and (c) the diffusion coefficient at the loss cone determines j_{prec}/j_{trap} ratio (Kennel & Petschek, 1966; Li et al., 2013). Thus, the energy spectrum of j_{prec}/j_{trap} is primarily determined by the wave intensity profile along magnetic field lines.

On the dayside, the simulated energy spectra of j_{prec}/j_{trap} agree reasonably well with observations: Figure 2 shows that in four out of six events, the simulated precipitation ratio energy profile is quite similar to the observations. In those cases, the empirical whistler-mode wave distribution agrees well with the instantaneous latitudinal profile of wave power, including at mid-to-high latitudes (Agapitov et al., 2018). The upper energy limit of precipitating

electrons is dictated by the maximum energy of trapped electrons that has sufficient flux to result in precipitation above the sensitivity level of the instrument. In other words, test-particle simulations with a trapped spectrum up to 1 MeV always have a longer energy tail of j_{prec}/j_{trap} ratio than the observed j_{prec}/j_{trap} ratio. The examples shown in Figure 2 suggest that the wave power distribution model qualitatively agrees with observations.

The same figure shows that the observed j_{prec}/j_{trap} profiles extend up to 500−700 keV. Scattering such energies requires that waves propagate to at least ∼30° in latitude (see, e.g., Artemyev et al., 2021). As the dayside latitudinal distribution of whistler-mode waves exhibits significant wave intensity at midlatitudes (Agapitov et al., 2018), it makes sense to observe relativistic electron scattering in this *MLT* sector (Thorne et al., 2005).

Figure 2f shows a questionable case, where the spectral slope of the precipitating flux ratio consistently underestimates ELFIN observations beyond uncertainty. Such discrepancy could be due to differences in the assumptions made regarding equatorial plasma conditions, or it could possibly be resolved by a minor corrective wave power increase at higher latitudes. On the other hand, Figure 2d shows a stark difference between simulation and observation with very strong j_{prec}/j_{trap} ratio (∼0.5) at relativistic energies (∼500 keV). Such strong precipitation cannot be described by a statistically averaged wave intensity model, and requires nearly constant wave amplitude up to midlatitudes, that is, possibly ducted waves (see discussion of similar ELFIN observations in Artemyev et al. (2021) and Tsai et al. (2022)). In both cases, the discrepancy is quite evident at energies >200 keV.

Figure 3 shows six examples of ELFIN observations of nightside relativistic electron precipitation. The nightside magnetosphere has a large population of suprathermal electrons (Li et al., 2010; Walsh et al., 2020) which quickly damp the waves when they propagate off their equatorial source location if they become oblique there. As a result, the observed wave power distribution exhibits a rapid decay with distance from the equator (or equivalently, with latitude along field lines) in this *MLT* sector (Meredith et al., 2012). Therefore, only ELFIN events with a rapid falloff of their precipitation ratio with energy can be consistent with the results of our simulations that rely on the statistical models of the above wave power distributions (as is the case for only one of the six nightside events, shown in Figure 3c). Three other nightside events (Figures 3a and 3d) show excessive precipitation at >200 keV; the j_{prec}/j_{trap} ratio for these events clearly deviates from expectation based on the simulation results for the aforementioned reason.

The remaining two events (Figures 3e and 3f) show excessive precipitation with $j_{prec}/j_{trap} \sim 1$ up to 400 and 800 keV, respectively. These events certainly cannot be described by the statistically averaged wave power distribution that we assumed. The event in 3f is the same as that in Figure 1b, where the ratio exceeding 1 can be seen in the context of the rest of the radiation belt crossing. When $j_{prec}/j_{trap} > 1$ at >300 keV, this is usually indicative of subspin electron flux variations, where the time difference of ∼0.7 s between precipitating and trapped flux measurements is longer than the timescale of the flux variation. Indeed, looking at subspin data confirms that multiple microbursts are included in this particular observation, which is not included in statistical results in Section 5 below due to the precipitating-to-trapped flux ratio increasing with energy (see Figure 1 in Zhang, Angelopoulos, et al. (2022), for another example of multiple microbursts in a single ELFIN science zone crossing).

Figures 2 and 3 demonstrate that statistical averages of wave power distribution (Agapitov et al., 2018) can reasonably describe most dayside relativistic electron precipitation and nightside subrelativistic (<200 keV) electron precipitation. The primary differences between simulations and observations occur for extreme events; that is, those with relativistic energies, either having $j_{prec}/j_{trap} > 0.5$ at dayside or $j_{prec}/j_{trap} > 0.1$ on nightside. These events could be explained by wave propagation with anomalously high wave intensity at midlatitudes, which is possible either through ducting or through equatorial generation with moderately oblique wave normal angles at the equator and subsequent refraction toward field-aligned propagation at higher latitudes (e.g., L. Chen et al., 2022; Miyoshi et al., 2020).

5. Statistical Results

To confirm the generality of the conclusions drawn from Figures 2 and 3, we compare test-particle simulations for three *MLT* sectors and two *L* shell ranges ($L \in [4, 5]$ and $L \in [5, 7]$) with statistically averaged ELFIN precipitating-to-trapped flux ratio observations. Since the empirical wave model has discrete bins, we pick a single *MLT*/*L* shell for modeling which represents that particular function of $B_w(\lambda)$ from the associated *MLT*/*L* bin. Figure 4 shows j_{prec}/j_{trap} profiles for the three *MLT* sectors: dawn-noon ($MLT \in [4, 13]$), noon-dusk ($MLT \in [13, 18]$), and night ($MLT \in [18, 24]$ or $\in [0, 4]$). ELFIN measurements are also separated by geomagnetic activity:

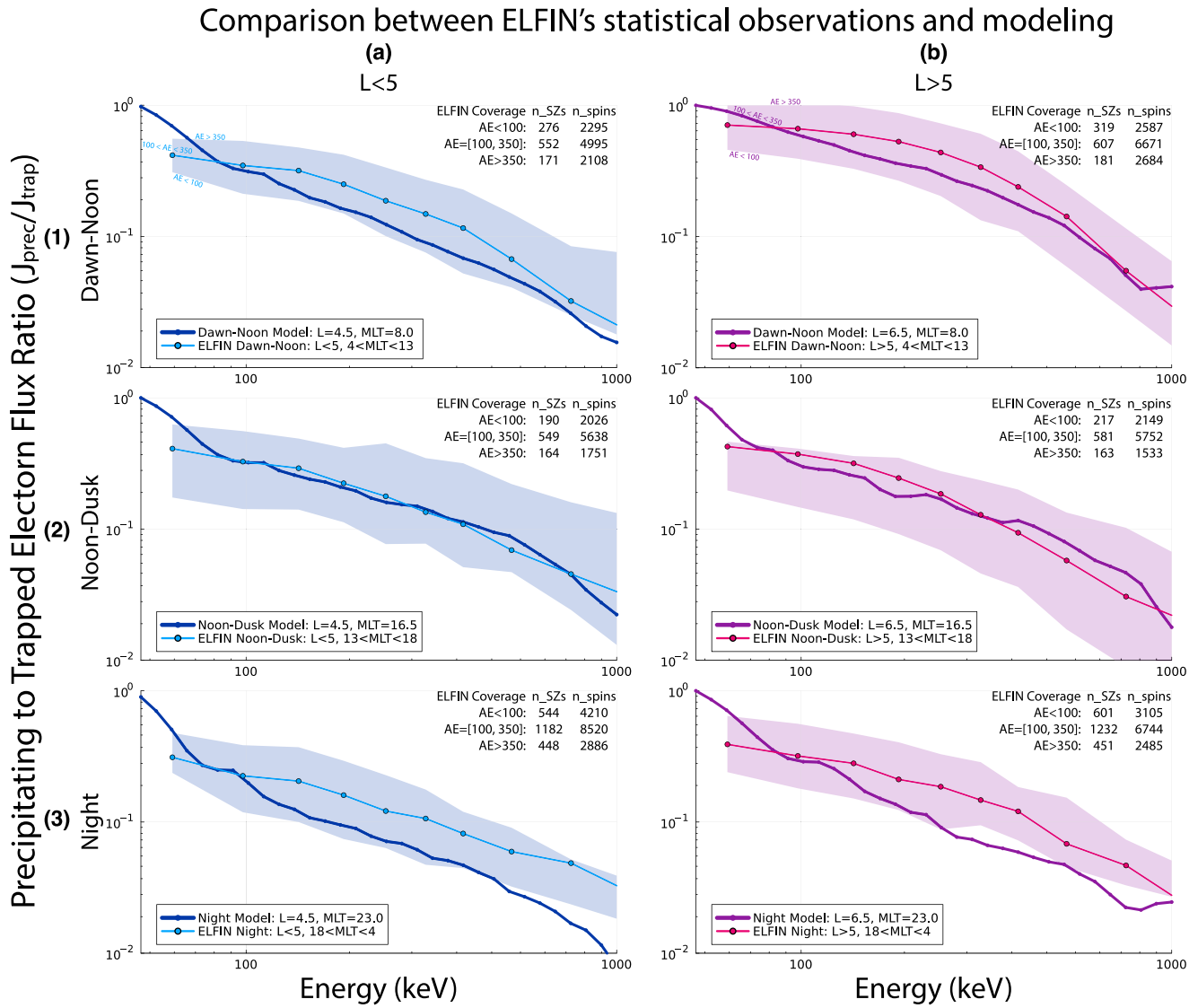

Figure 4. Rows (1), (2), and (3) show model/observation comparisons of normalized precipitating energy spectra at three different *MLT* sectors, whereas columns (a) and (b) show model/observation comparisons at either low or high *L* shells. Each plot uses light blue (Electron Losses and Fields INvestgation (ELFIN) observations) and dark blue (model) at low *L* shells plus magenta (ELFIN observations) and purple (model) at high *L* shells. Shaded regions represent boundaries of low ($AE < 100$ nT) and high ($AE > 350$ nT) geomagnetic activity. The statistical coverage used for the ELFIN data is shown in Figure 5. Modeled precipitation is consistent with observations for the dusk *MLT* sector ($13 < MLT < 18$) and high *L* shells on the dawn/dayside ($4 < MLT < 13$). However, there is a slight underestimation at lower *L* shells on the dawn/day side above 200 keV, while the deviation becomes much more significant at all *L* shells on the nightside.

low ($AE < 100$ nT), medium ($100\ \text{nT} < AE < 350$ nT), and high ($AE > 350$ nT). This is indicated by the light shading enveloping the solid lines marked with outlined circles: the center lines denote the moderate activity level, whereas the low and high activity levels are denoted by the lower and upper bounds of the shaded region—they can be considered as an uncertainty range for the ELFIN-observed precipitation rates. The breakdown of the statistical coverage of ELFIN data used for this study is summarized in Figure 5. Like before, we use the same normalization of j_{prec}/j_{trap} at 80 keV to the medium geomagnetic activity ELFIN curve, however, to increase consistency of statistics in the simulation, we increase the number of particles in each simulation ensemble to $N = 1e6$.

Simulation results do a decent job describing the statistically averaged precipitation rate for dawn-noon at high *L* shells (Figure 4.1b) and noon-dusk (Figure 4.2). For low *L* shells on the dawn-noon sector (Figure 4.1a), the empirical wave power distribution as a function of latitude decreases too quickly, and thus the simulated precipitation rates slightly underestimate the observed scattering rates. Similar to the dayside case studies in Figure 2,

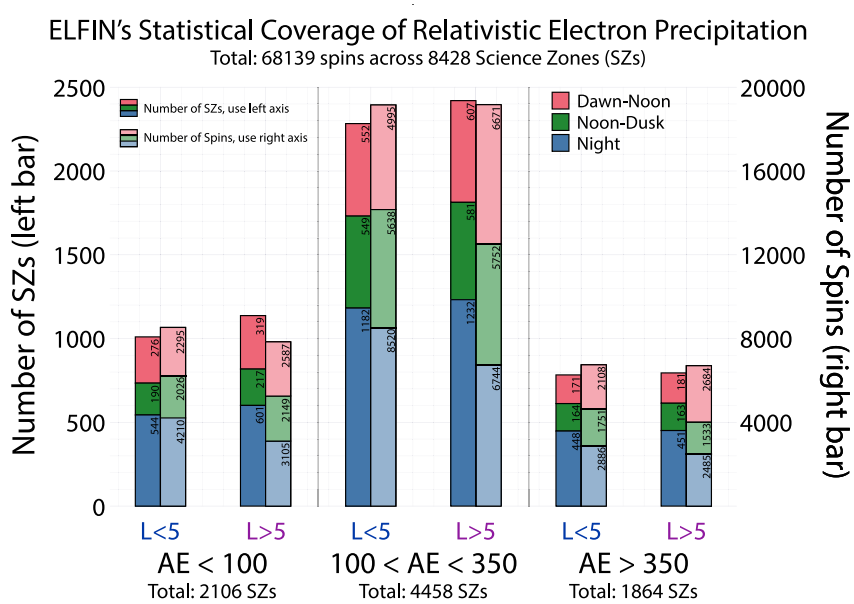

Figure 5. Electron Losses and Fields INvestgation's (ELFIN) data coverage of energetic bursty electron precipitation over a ~1 year period utilized in Figure 4's statistical averages, broken down into instantaneous *AE* disturbance levels and low/high *L* shells (shown by each individual bar graph) as well as *MLT* sector (shown by stacked bars). Left bars/primary axis show number of science zones (SZs) (i.e., radiation belt crossings) while right bars/secondary axis show the number of spins that actually constituted the empirical average. Note that field-line curvature scattering and EMIC-driven precipitation was excluded from this data set.

this minor underestimation is most apparent ~200 keV. However, in the nightside *MLT* sector (Figure 4.3), the discrepancy between simulations and observations is most apparent: test-particle simulations suggest a steep precipitation rate decrease with energy, whereas ELFIN observations show statistically important losses of relativistic electrons. This discrepancy cannot be attributed to curvature scattering (which can also increase relativistic electron precipitation on the nightside during active times, see, e.g., ELFIN observation analysis in Artemyev, Angelopoulos, et al. (2022)), because we took provisions to specifically exclude all j_{prec}/j_{trap} profiles showing curvature scattering features from the data set (i.e., those with increasing j_{prec}/j_{trap} with energy at lower *L* shells, see discussion of such features in Sergeev et al. (1993) and Dubyagin et al. (2002)). Therefore, there are two potential main sources for the aforementioned simulation-observation discrepancy: (a) relativistic electron scattering by intense, bursty, field-aligned, mid-to-high-latitude nightside whistler-mode waves which are currently unaccounted for in statistical wave models or (b) uncertainties of ELFIN orbit projections onto the equatorial plane (the uncertainties of such projections are expected to be largest on the nightside due to how stretched magnetic field lines are during substorm activity). To address the latter issue, we checked that Figure 4 did not significantly change between the usage of the default nonstorm magnetic field model used (Tsyganenko, 1989) and a more accurate model (Tsyganenko, 1995). Note that we did not use the storm-time model (Tsyganenko & Sitnov, 2005) because the majority of our observations events are not associated with storm activity. The primary uncertainty in nightside projections should be attributed to substorm dynamics with the formation of the thin current sheet along with very strong magnetic field-line stretching (see examples and discussion in Artemyev, Angelopoulos, et al. (2022)). Such dynamics may be better handled by more advanced magnetic field models (such as, e.g., Sitnov et al., 2019; Stephens et al., 2019), and thus, it may be a good idea to revisit ELFIN projections during substorm dynamics when such models become publicly available.

A less likely possibility, to be discussed in Section 6, is very oblique, near-equatorial chorus that results in relativistic electron precipitation due to high-order resonances (recently discussed using the ELFIN data set in Gan et al. (2023)), though the resulting flux ratio energy-spectra in their case study appears different from the measured ones presented herein. Regardless, Figure 4 statistically validates our multicase-study results from Figures 2 and 3: the simulated energetic (subrelativistic and relativistic) precipitation ratio as a function of energy inferred from statistical averages of the whistler-mode wave power distribution agrees reasonably well with observations of precipitation at the dawn-noon-dusk *MLT* sector (except during strong relativistic precipitation events), as well

as at the nightside for subrelativistic energies, but seems to consistently underestimate relativistic precipitation on the nightside.

6. Discussion and Conclusions

In this paper, we have shown that low-altitude observations of precipitating electron energy spectra can often contain more energetic losses than would be expected from electron scattering by typical (i.e., statistically averaged) whistler-mode wave amplitudes. In both our case and statistical studies, we selected only events with unambiguous signatures of whistler-driven precipitation. Specifically, we excluded events exhibiting electron precipitation due to field-line curvature scattering (based on their dispersive energy signature) or electromagnetic ion cyclotron (EMIC) waves (based on their increasing precipitating-to-trapped ratio with energy, peaking at relativistic energies). Modern radiation belt simulation and modeling tools mostly rely on EMIC-driven electron precipitation to explain relativistic electron losses (see, e.g., Drozdov et al., 2017; Ma et al., 2015; and references therein), partly because whistler-mode wave models cannot provide sufficiently large rates of relativistic electron scattering. Our results indicate, however, that inclusion of higher wave power at mid-to-high latitudes (e.g., due to ducted whistler-mode waves or moderately oblique source whistlers that become field-aligned away from the equator due to refraction; see, e.g., Breuillard et al., 2012; L. Chen et al., 2013; Watt et al., 2013) could appreciably enhance the contribution of whistler-mode waves to relativistic electron scattering. Thus, EMIC waves may not be unique in their ability to scatter relativistic electrons (especially those $\lesssim$1 MeV, which are at the limit of the expected minimum EMIC-wave resonance energy in typical inner magnetosphere density and magnetic field conditions; see discussions regarding the importance of EMIC-driven scattering of $\lesssim$1 MeV in L. Chen et al. (2016), Capannolo et al. (2019), Hendry et al. (2017), and Bashir et al. (2022)).

The question then arises: if mid-to-high-latitude whistler-mode waves are important, how can we quantify this population of waves in the radiation belt? Simultaneous equatorial and midlatitude observations of whistler-mode waves require multispacecraft wave measurements and are quite rare (e.g., Colpitts et al., 2020). Realistic ray tracing simulations (Bortnik et al., 2007; L. Chen et al., 2013; Katoh, 2014; Watt et al., 2013) require detailed information about suprathermal electron populations and their anisotropy (see discussion in Bortnik et al. (2006), Li et al. (2010), and Ma et al. (2017)). Ground-based VLF wave observations (which are often associated with ducted whistler-mode wave propagation to the ionosphere, see Demekhov et al., 2020; Douma et al., 2018; Martinez-Calderon et al., 2015; Simms et al., 2019; Titova et al., 2015) capture only some of the fully ducted waves that reach the ground and clearly cannot cover those that only reach midlatitudes. This study suggests a new approach for performing such investigations, which may involve a statistical investigation of electron precipitating spectra, where <100 keV fluxes can be attributed to equatorial whistler-mode waves (Li et al., 2013, 2014; Ni et al., 2014), while >200 keV fluxes can be associated with the latitudinal profiles of the whistler-mode wave intensity (see discussion in Artemyev et al., 2021; Zhang, Angelopoulos, et al., 2022). However, recent theoretical and observational work suggests that very oblique (nearly electrostatic) whistler-mode waves can also effectively scatter electrons up to several hundreds of keV (see Li et al., 2014; Lorentzen et al., 2001; Mourenas et al., 2014). This explanation is less likely for two reasons: (a) oblique waves are significantly less efficient at scattering electrons beyond 200 keV in comparison with 50 keV electrons (e.g., Artemyev, Zhang, et al., 2022; Gan et al., 2023) and (b) electron scattering via oblique waves are statistically less efficient on the nightside as compared to the dayside (e.g., Aryan et al., 2020, and references therein), the latter of which contradicts this study's findings. Regardless, the potential of bursty oblique waves that are smoothed out in statistically averaged models cannot be entirely discarded, so the aforementioned approach alone cannot separate the contributions to relativistic electron precipitation by intense, field-aligned, midlatitude whistler-mode waves from those by intense, highly oblique, near-equatorial whistler-mode waves. A preliminary look at published observational and modeled flux ratio energy spectra suggest that the spectral slope of j_{prec}/j_{trap} due to oblique whistler-electron high-order resonance interactions may be steeper than the case studies presented in this paper (i.e., scattering by near-equatorial oblique waves is less efficient at higher energies). Careful examination of that process, including its pitch angle spectra, may allow us to disambiguate its relative contribution to the global relativistic precipitation from that of ducted waves. Furthermore, accurate quantitative estimation of the relative contribution of ducted whistler-mode waves to mid-to-high-latitude wave power (and thus to relativistic electron scattering and losses) requires careful, detailed studies of low-altitude energy and pitch angle electron flux spectra combined with either conjugate equatorial wave measurements (see cases studies in Capannolo et al. (2018), Shi et al. (2022), and Zhang,

Artemyev, et al. (2022)) or local (i.e., low-altitude, see examples in Benck et al. (2008), Hayosh et al. (2013), and Shen et al. (2021)) wave measurements.

In summary, we compared ELFIN energy spectra of energetic electron precipitation-to-trapped flux ratios due to pitch angle scattering by nonlinear interactions with whistler-mode waves with expected precipitation spectra using test-particle simulations of such scattering by empirical models of wave power distributions of whistler-mode waves. The results suggest that these empirical models are inconsistent with the observed relativistic electron precipitation by such waves on the nightside, and occasionally also inconsistent with observed precipitation on the dayside. The discrepancy between the observed average wave power distribution and observed precipitation spectra was further reinforced by simulation comparisons with statistical averages of ELFIN observations using 2 years of data at three local time sectors. One way to resolve this discrepancy is by incorporating the contribution of intense, field-aligned waves capable of propagating to midlatitudes. However, further investigations are needed to clarify the relative occurrence rate of relativistic electron precipitation events due to midlatitude whistler-wave propagation and the overall contribution of such waves to the dynamic evolution of the outer radiation belt.

Data Availability Statement

ELFIN data are available at https://data.elfin.ucla.edu/ and online summary plots at https://plots.elfin.ucla.edu/summary.php.
Data access and processing was done using SPEDAS V4.1, see Angelopoulos et al. (2019).
Test-particle simulation code is found at https://github.com/ethantsai/nlwhistlers (Tsai, 2023).

Acknowledgments
We acknowledge support by NASA award 80NSSC23K0089, 80NSSC22K0522 and NSF Grants NSF-2026375, AGS-1242918, AGS-2019950, and AGS-2021749. We are grateful to NASA's CubeSat Launch Initiative and Launch Services Program for ELFIN's successful launch in the desired orbits. We acknowledge early support of ELFIN project by the AFOSR, under its University Nanosat Program, UNP-8 project, contract FA9453-12-D-0285, and by the California Space Grant program. Importantly, we graciously acknowledge the critical contributions by numerous UCLA students who made the ELFIN mission a success. We also acknowledge that the Kp indices used throughout this study were provided by the WDC for Geomagnetism, Kyoto (http://wdc.kugi.kyoto-u.ac.jp/wdc/Sec3.html) and GFZ Helmholtz Centre Potsdam (https://kp.gfz-potsdam.de/en/).

References

Agapitov, O. V., Artemyev, A., Krasnoselskikh, V., Khotyaintsev, Y. V., Mourenas, D., Breuillard, H., et al. (2013). Statistics of whistler mode waves in the outer radiation belt: Cluster STAFF-SA measurements. *Journal of Geophysical Research*, *118*, 3407–3420. https://doi.org/10.1002/jgra.50312

Agapitov, O. V., Mourenas, D., Artemyev, A. V., Mozer, F. S., Hospodarsky, G., Bonnell, J., & Krasnoselskikh, V. (2018). Synthetic empirical chorus wave model from combined Van Allen Probes and Cluster statistics. *Journal of Geophysical Research: Space Physics*, *123*, 297–314. https://doi.org/10.1002/2017JA024843

Albert, J. M. (2001). Comparison of pitch angle diffusion by turbulent and monochromatic whistler waves. *Journal of Geophysical Research*, *106*(A5), 8477–8482. https://doi.org/10.1029/2000JA000304

Albert, J. M. (2010). Diffusion by one wave and by many waves. *Journal of Geophysical Research*, *115*, A00F05. https://doi.org/10.1029/2009JA014732

Albert, J. M. (2017). Quasi-linear diffusion coefficients for highly oblique whistler mode waves. *Journal of Geophysical Research*, *122*, 5339–5354. https://doi.org/10.1002/2017JA024124

Albert, J. M., Artemyev, A. V., Li, W., Gan, L., & Ma, Q. (2021). Models of resonant wave-particle interactions. *Journal of Geophysical Research: Space Physics*, *126*, e2021JA029216. https://doi.org/10.1029/2021JA029216

Albert, J. M., Tao, X., & Bortnik, J. (2013). Aspects of nonlinear wave-particle interactions. In D. Summers, I. U. Mann, D. N. Baker, & M. Schulz (Eds.), *Dynamics of the earth's radiation belts and inner magnetosphere* (pp. 255–264). American Geophysical Union. https://doi.org/10.1029/2012GM001324

Allison, H. J., & Shprits, Y. Y. (2020). Local heating of radiation belt electrons to ultra-relativistic energies. *Nature Communications*, *11*(1), 4533. https://doi.org/10.1038/s41467-020-18053-z

An, Z., Wu, Y., & Tao, X. (2022). Electron dynamics in a chorus wave field generated from particle-in-cell simulations. *Geophysical Research Letters*, *49*, e97778. https://doi.org/10.1029/2022GL097778

Angelopoulos, V., Cruce, P., Drozdov, A., Grimes, E. W., Hatzigeorgiu, N., King, D. A., et al. (2019). The space physics environment data analysis system (SPEDAS). *Space Science Reviews*, *215*(1), 9. https://doi.org/10.1007/s11214-018-0576-4

Angelopoulos, V., Tsai, E., Bingley, L., Shaffer, C., Turner, D. L., Runov, A., et al. (2020). The ELFIN mission. *Space Science Reviews*, *216*(5), 103. https://doi.org/10.1007/s11214-020-00721-7

Angelopoulos, V., Zhang, X. J., Artemyev, A. V., Mourenas, D., Tsai, E., Wilkins, C., et al. (2022). Energetic electron precipitation driven by electromagnetic ion cyclotron waves from ELFIN's low altitude perspective. *arXiv e-prints*, arXiv:2211.15653. https://doi.org/10.48550/arXiv.2211.15653

Artemyev, A. V., Agapitov, O., Mourenas, D., Krasnoselskikh, V., Shastun, V., & Mozer, F. (2016). Oblique whistler-mode waves in the earth's inner magnetosphere: Energy distribution, origins, and role in radiation belt dynamics. *Space Science Reviews*, *200*(1–4), 261–355. https://doi.org/10.1007/s11214-016-0252-5

Artemyev, A. V., Angelopoulos, V., Zhang, X. J., Runov, A., Petrukovich, A., Nakamura, R., et al. (2022). Thinning of the magnetotail current sheet inferred from low-altitude observations of energetic electrons. *Journal of Geophysical Research: Space Physics*, *127*, e2022JA030705. https://doi.org/10.1029/2022JA030705

Artemyev, A. V., Demekhov, A. G., Zhang, X. J., Angelopoulos, V., Mourenas, D., Fedorenko, Y. V., et al. (2021). Role of ducting in relativistic electron loss by whistler-mode wave scattering. *Journal of Geophysical Research: Space Physics*, *126*, e29851. https://doi.org/10.1029/2021JA029851

Artemyev, A. V., Zhang, X. J., Zou, Y., Mourenas, D., Angelopoulos, V., Vainchtein, D., et al. (2022). On the nature of intense sub-relativistic electron precipitation. *Journal of Geophysical Research: Space Physics*, *127*, e30571. https://doi.org/10.1029/2022JA030571

Aryan, H., Agapitov, O. V., Artemyev, A., Mourenas, D., Balikhin, M. A., Boynton, R., & Bortnik, J. (2020). Outer radiation belt electron Lifetime model based on combined Van Allen Probes and Cluster VLF measurements. *Journal of Geophysical Research: Space Physics*, *125*, e28018. https://doi.org/10.1029/2020JA028018

Bashir, M. F., Artemyev, A., Zhang, X.-J., & Angelopoulos, V. (2022). Hot plasma effects on electron resonant scattering by electromagnetic ion cyclotron waves. *Geophysical Research Letters*, *49*, e99229. https://doi.org/10.1029/2022GL099229

Bell, T. F. (1984). The nonlinear gyroresonance interaction between energetic electrons and coherent VLF waves propagating at an arbitrary angle with respect to the earth's magnetic field. *Journal of Geophysical Research*, *89*(A2), 905–918. https://doi.org/10.1029/JA089iA02p00905

Bell, T. F., Inan, U. S., Bortnik, J., & Scudder, J. D. (2002). The Landau damping of magnetospherically reflected whistlers within the plasmasphere. *Geophysical Research Letters*, *29*(15), 1733. https://doi.org/10.1029/2002GL014752

Benck, S., Cyamukungu, M., & Cabrera, J. (2008). Study of correlations between waves and particle fluxes measured on board the DEMETER satellite. *Advances in Space Research*, *42*(9), 1538–1549. https://doi.org/10.1016/j.asr.2008.03.024

Bezanson, J., Edelman, A., Karpinski, S., & Shah, V. B. (2017). Julia: A fresh approach to numerical computing. *SIAM Review*, *59*(1), 65–98. https://doi.org/10.1137/141000671

Blum, L. W., Li, X., & Denton, M. (2015). Rapid MeV electron precipitation as observed by SAMPEX/HILT during high-speed stream-driven storms. *Journal of Geophysical Research: Space Physics*, *120*, 3783–3794. https://doi.org/10.1002/2014JA020633

Bortnik, J., Inan, U. S., & Bell, T. F. (2006). Landau damping and resultant unidirectional propagation of chorus waves. *Geophysical Research Letters*, *33*, L03102. https://doi.org/10.1029/2005GL024553

Bortnik, J., & Thorne, R. M. (2007). The dual role of ELF/VLF chorus waves in the acceleration and precipitation of radiation belt electrons. *Journal of Atmospheric and Solar-Terrestrial Physics*, *69*(3), 378–386. https://doi.org/10.1016/j.jastp.2006.05.030

Bortnik, J., Thorne, R. M., & Inan, U. S. (2008). Nonlinear interaction of energetic electrons with large amplitude chorus. *Geophysical Research Letters*, *35*, L21102. https://doi.org/10.1029/2008GL035500

Bortnik, J., Thorne, R. M., Meredith, N. P., & Santolik, O. (2007). Ray tracing of penetrating chorus and its implications for the radiation belts. *Geophysical Research Letters*, *34*, L15109. https://doi.org/10.1029/2007GL030040

Breneman, A. W., Crew, A., Sample, J., Klumpar, D., Johnson, A., Agapitov, O., et al. (2017). Observations directly linking relativistic electron microbursts to whistler mode chorus: Van Allen Probes and FIREBIRD II. *Geophysical Research Letters*, *44*, 11265–11272. https://doi.org/10.1002/2017GL075001

Breuillard, H., Zaliznyak, Y., Krasnoselskikh, V., Agapitov, O., Artemyev, A., & Rolland, G. (2012). Chorus wave-normal statistics in the Earth's radiation belts from ray tracing technique. *Annales Geophysicae*, *30*(8), 1223–1233. https://doi.org/10.5194/angeo-30-1223-2012

Capannolo, L., Li, W., Ma, Q., Chen, L., Shen, X. C., Spence, H. E., et al. (2019). Direct observation of subrelativistic electron precipitation potentially driven by EMIC waves. *Geophysical Research Letters*, *46*, 12711–12721. https://doi.org/10.1029/2019GL084202

Capannolo, L., Li, W., Ma, Q., Qin, M., Shen, X. C., Angelopoulos, V., et al. (2023). Electron precipitation observed by elfin using proton precipitation as a proxy for electromagnetic ion cyclotron (emic) waves. *Geophysical Research Letters*, *50*, e2022GL102133. https://doi.org/10.1029/2023GL103519

Capannolo, L., Li, W., Ma, Q., Zhang, X.-J., Redmon, R. J., Rodriguez, J. V., et al. (2018). Understanding the driver of energetic electron precipitation using coordinated multisatellite measurements. *Geophysical Research Letters*, *45*, 6755–6765. https://doi.org/10.1029/2018GL078604

Chen, L., Thorne, R. M., Bortnik, J., & Zhang, X.-J. (2016). Nonresonant interactions of electromagnetic ion cyclotron waves with relativistic electrons. *Journal of Geophysical Research: Space Physics*, *121*, 9913–9925. https://doi.org/10.1002/2016JA022813

Chen, L., Thorne, R. M., Li, W., & Bortnik, J. (2013). Modeling the wave normal distribution of chorus waves. *Journal of Geophysical Research: Space Physics*, *118*, 1074–1088. https://doi.org/10.1029/2012JA018343

Chen, L., Zhang, X.-J., Artemyev, A., Angelopoulos, V., Tsai, E., Wilkins, C., & Horne, R. B. (2022). Ducted chorus waves cause sub-relativistic and relativistic electron microbursts. *Geophysical Research Letters*, *49*, e97559. https://doi.org/10.1029/2021GL097559

Chen, R., Gao, X., Lu, Q., Chen, L., Tsurutani, B. T., Li, W., & Wang, S. (2021). In situ observations of whistler mode chorus waves guided by density ducts. *Journal of Geophysical Research: Space Physics*, *126*, e28814. https://doi.org/10.1029/2020JA028814

Colpitts, C., Miyoshi, Y., Kasahara, Y., Delzanno, G. L., Wygant, J. R., Cattell, C. A., et al. (2020). First direct observations of propagation of discrete chorus elements from the equatorial source to higher latitudes, using the Van Allen Probes and Arase satellites. *Journal of Geophysical Research: Space Physics*, *125*, e28315. https://doi.org/10.1029/2020JA028315

Demekhov, A. G. (2011). Generation of VLF emissions with the increasing and decreasing frequency in the magnetosperic cyclotron maser in the backward wave oscillator regime. *Radiophysics and Quantum Electronics*, *53*(11), 609–622. https://doi.org/10.1007/s11141-011-9256-x

Demekhov, A. G., Manninen, J., Santolík, O., & Titova, E. E. (2017). Conjugate ground-spacecraft observations of VLF chorus elements. *Geophysical Research Letters*, *44*, 11735–11744. https://doi.org/10.1002/2017GL076139

Demekhov, A. G., Titova, E. E., Maninnen, J., Pasmanik, D. L., Lubchich, A. A., Santolík, O., et al. (2020). Localization of the source of Quasiperiodic VLF emissions in the magnetosphere by using simultaneous ground and space observations: A case study. *Journal of Geophysical Research: Space Physics*, *125*, e27776. https://doi.org/10.1029/2020JA027776

Demekhov, A. G., Trakhtengerts, V. Y., Rycroft, M. J., & Nunn, D. (2006). Electron acceleration in the magnetosphere by whistler-mode waves of varying frequency. *Geomagnetism and Aeronomy*, *46*(6), 711–716. https://doi.org/10.1134/S0016793206060053

Denton, R. E., Takahashi, K., Galkin, I. A., Nsumei, P. A., Huang, X., Reinisch, B. W., et al. (2006). Distribution of density along magnetospheric field lines. *Journal of Geophysical Research*, *111*, A04213. https://doi.org/10.1029/2005JA011414

Douma, E., Rodger, C. J., Blum, L. W., O'Brien, T. P., Clilverd, M. A., & Blake, J. B. (2019). Characteristics of relativistic microburst intensity from SAMPEX observations. *Journal of Geophysical Research: Space Physics*, *124*, 5627–5640. https://doi.org/10.1029/2019JA026757

Douma, E., Rodger, C. J., Clilverd, M. A., Hendry, A. T., Engebretson, M. J., & Lessard, M. R. (2018). Comparison of relativistic microburst activity seen by SAMPEX with ground-based wave measurements at Halley, Antarctica. *Journal of Geophysical Research: Space Physics*, *123*, 1279–1294. https://doi.org/10.1002/2017JA024754

Drozdov, A. Y., Shprits, Y. Y., Usanova, M. E., Aseev, N. A., Kellerman, A. C., & Zhu, H. (2017). EMIC wave parameterization in the long-term VERB code simulation. *Journal of Geophysical Research: Space Physics*, *122*, 8488–8501. https://doi.org/10.1002/2017JA024389

Dubyagin, S., Sergeev, V. A., & Kubyshkina, M. V. (2002). On the remote sensing of plasma sheet from low-altitude spacecraft. *Journal of Atmospheric and Solar-Terrestrial Physics*, *64*(5–6), 567–572. https://doi.org/10.1016/S1364-6826(02)00014-7

Gan, L., Artemyev, A., Li, W., Zhang, X.-J., Ma, Q., Mourenas, D., et al. (2023). Bursty energetic electron precipitation by high-order resonance with very-oblique whistler-mode waves. *Geophysical Research Letters*, *50*, e2022GL101920. https://doi.org/10.1029/2022GL101920

Grach, V. S., Artemyev, A. V., Demekhov, A. G., Zhang, X.-J., Bortnik, J., Angelopoulos, V., et al. (2022). Relativistic electron precipitation by EMIC waves: Importance of nonlinear resonant effects. *Geophysical Research Letters*, *49*, e99994. https://doi.org/10.1029/2022GL099994

Hanzelka, M., & Santolík, O. (2019). Effects of ducting on whistler mode chorus or Exohiss in the outer radiation belt. *Geophysical Research Letters*, *46*, 5735–5745. https://doi.org/10.1029/2019GL083115

Hanzelka, M., & Santolík, O. (2022). Effects of field-aligned cold plasma density filaments on the fine structure of chorus. *Geophysical Research Letters*, *49*, e2022GL101654. https://doi.org/10.1029/2022GL101654

Hayosh, M., Pasmanik, D. L., Demekhov, A. G., Santolik, O., Parrot, M., & Titova, E. E. (2013). Simultaneous observations of quasi-periodic ELF/VLF wave emissions and electron precipitation by DEMETER satellite: A case study. *Journal of Geophysical Research: Space Physics*, *118*, 4523–4533. https://doi.org/10.1002/jgra.50179

Helliwell, R. A. (1965). *Whistlers and related ionospheric phenomena*. Stanford University Press.

Hendry, A. T., Rodger, C. J., & Clilverd, M. A. (2017). Evidence of sub-MeV EMIC-driven electron precipitation. *Geophysical Research Letters*, *44*, 1210–1218. https://doi.org/10.1002/2016GL071807

Hosseini, P., Agapitov, O., Harid, V., & Gołkowski, M. (2021). Evidence of small scale plasma Irregularity effects on whistler mode chorus propagation. *Geophysical Research Letters*, *48*, e92850. https://doi.org/10.1029/2021GL092850

Kang, N., Bortnik, J., Zhang, X., Claudepierre, S., & Shi, X. (2022). Relativistic microburst scale size induced by a single point-source chorus element. *Geophysical Research Letters*, *49*, e2022GL100841. https://doi.org/10.1029/2022GL100841

Karpman, V. I., & Kaufman, R. N. (1982). Whistler wave propagation in density ducts. *Journal of Plasma Physics*, *27*(2), 225–238. https://doi.org/10.1017/S0022377800026556

Katoh, Y. (2014). A simulation study of the propagation of whistler-mode chorus in the Earth's inner magnetosphere. *Earth Planets and Space*, *66*(1), 6. https://doi.org/10.1186/1880-5981-66-6

Katoh, Y., & Omura, Y. (2007). Computer simulation of chorus wave generation in the Earth's inner magnetosphere. *Geophysical Research Letters*, *34*, L03102. https://doi.org/10.1029/2006GL028594

Katoh, Y., Omura, Y., & Summers, D. (2008). Rapid energization of radiation belt electrons by nonlinear wave trapping. *Annales Geophysicae*, *26*(11), 3451–3456. https://doi.org/10.5194/angeo-26-3451-2008

Kennel, C. F., & Petschek, H. E. (1966). Limit on stably trapped particle fluxes. *Journal of Geophysical Research*, *71*, 1–28. https://doi.org/10.1029/jz071i001p00001

Kitahara, M., & Katoh, Y. (2019). Anomalous trapping of low pitch angle electrons by coherent whistler mode waves. *Journal of Geophysical Research: Space Physics*, *124*, 5568–5583. https://doi.org/10.1029/2019JA026493

Li, W., Bortnik, J., Thorne, R. M., & Angelopoulos, V. (2011). Global distribution of wave amplitudes and wave normal angles of chorus waves using THEMIS wave observations. *Journal of Geophysical Research*, *116*, A12205. https://doi.org/10.1029/2011JA017035

Li, W., Mourenas, D., Artemyev, A., Agapitov, O., Bortnik, J., Albert, J., et al. (2014). Evidence of stronger pitch angle scattering loss caused by oblique whistler-mode waves as compared with quasi-parallel waves. *Geophysical Research Letters*, *41*, 6063–6070. https://doi.org/10.1002/2014GL061260

Li, W., Ni, B., Thorne, R. M., Bortnik, J., Green, J. C., Kletzing, C. A., et al. (2013). Constructing the global distribution of chorus wave intensity using measurements of electrons by the POES satellites and waves by the Van Allen Probes. *Geophysical Research Letters*, *40*, 4526–4532. https://doi.org/10.1002/grl.50920

Li, W., Thorne, R. M., Bortnik, J., Nishimura, Y., Angelopoulos, V., Chen, L., et al. (2010). Global distributions of suprathermal electrons observed on THEMIS and potential mechanisms for access into the plasmasphere. *Journal of Geophysical Research*, *115*, A00J10. https://doi.org/10.1029/2010JA015687

Lorentzen, K. R., Blake, J. B., Inan, U. S., & Bortnik, J. (2001). Observations of relativistic electron microbursts in association with VLF chorus. *Journal of Geophysical Research*, *106*(A4), 6017–6028. https://doi.org/10.1029/2000JA003018

Lyons, L. R., & Williams, D. J. (1984). *Quantitative aspects of magnetospheric physics*. D. Reidel.

Ma, Q., Artemyev, A. V., Mourenas, D., Li, W., Thorne, R. M., Kletzing, C. A., et al. (2017). Very oblique whistler mode propagation in the radiation belts: Effects of Hot plasma and Landau damping. *Geophysical Research Letters*, *44*, 12057–12066. https://doi.org/10.1002/2017GL075892

Ma, Q., Li, W., Thorne, R. M., Ni, B., Kletzing, C. A., Kurth, W. S., et al. (2015). Modeling inward diffusion and slow decay of energetic electrons in the Earth's outer radiation belt. *Geophysical Research Letters*, *42*, 987–995. https://doi.org/10.1002/2014GL062977

Martinez-Calderon, C., Katoh, Y., Manninen, J., Kasahara, Y., Matsuda, S., Kumamoto, A., et al. (2020). Conjugate observations of dayside and nightside VLF chorus and QP emissions between Arase (ERG) and Kannuslehto, Finland. *Journal of Geophysical Research: Space Physics*, *125*, e26663. https://doi.org/10.1029/2019JA026663

Martinez-Calderon, C., Shiokawa, K., Miyoshi, Y., Keika, K., Ozaki, M., Schofield, I., et al. (2016). ELF/VLF wave propagation at subauroral latitudes: Conjugate observation between the ground and Van Allen Probes A. *Journal of Geophysical Research: Space Physics*, *121*, 5384–5393. https://doi.org/10.1002/2015JA022264

Martinez-Calderon, C., Shiokawa, K., Miyoshi, Y., Ozaki, M., Schofield, I., & Connors, M. (2015). Statistical study of ELF/VLF emissions at subauroral latitudes in Athabasca, Canada. *Journal of Geophysical Research: Space Physics*, *120*, 8455–8469. https://doi.org/10.1002/2015JA021347

Meredith, N. P., Horne, R. B., & Anderson, R. R. (2001). Substorm dependence of chorus amplitudes: Implications for the acceleration of electrons to relativistic energies. *Journal of Geophysical Research*, *106*(A7), 13165–13178. https://doi.org/10.1029/2000JA900156

Meredith, N. P., Horne, R. B., Iles, R. H. A., Thorne, R. M., Heynderickx, D., & Anderson, R. R. (2002). Outer zone relativistic electron acceleration associated with substorm-enhanced whistler mode chorus. *Journal of Geophysical Research*, *107*(A7), 1144. https://doi.org/10.1029/2001JA900146

Meredith, N. P., Horne, R. B., Sicard-Piet, A., Boscher, D., Yearby, K. H., Li, W., & Thorne, R. M. (2012). Global model of lower band and upper band chorus from multiple satellite observations. *Journal of Geophysical Research*, *117*, A10225. https://doi.org/10.1029/2012JA017978

Millan, R. M., & Baker, D. N. (2012). Acceleration of particles to high energies in earth's radiation belts. *Space Science Reviews*, *173*(1–4), 103–131. https://doi.org/10.1007/s11214-012-9941-x

Millan, R. M., & Thorne, R. M. (2007). Review of radiation belt relativistic electron losses. *Journal of Atmospheric and Solar-Terrestrial Physics*, *69*(3), 362–377. https://doi.org/10.1016/j.jastp.2006.06.019

Miyoshi, Y., Hosokawa, S., Kurita, S.-I., Oyama, Y., Ogawa, S., Saito, I., et al. (2021). Penetration of MeV electrons into the mesosphere accompanying pulsating aurorae. *Scientific Reports*, *11*(1), 13724. https://doi.org/10.1038/s41598-021-92611-3

Miyoshi, Y., Saito, S., Kurita, S., Asamura, K., Hosokawa, K., Sakanoi, T., et al. (2020). Relativistic electron microbursts as high-energy tail of pulsating Aurora electrons. *Geophysical Research Letters*, *47*, e90360. https://doi.org/10.1029/2020GL090360

Mourenas, D., Artemyev, A., Agapitov, O., & Krasnoselskikh, V. (2012). Acceleration of radiation belts electrons by oblique chorus waves. *Journal of Geophysical Research*, *117*, A10212. https://doi.org/10.1029/2012JA018041

Mourenas, D., Artemyev, A. V., Agapitov, O. V., & Krasnoselskikh, V. (2014). Consequences of geomagnetic activity on energization and loss of radiation belt electrons by oblique chorus waves. *Journal of Geophysical Research*, *119*, 2775–2796. https://doi.org/10.1002/2013JA019674

Mourenas, D., Artemyev, A. V., Zhang, X. J., & Angelopoulos, V. (2022). Extreme energy spectra of relativistic electron flux in the outer radiation belt. *Journal of Geophysical Research: Space Physics*, *127*, e2022JA031038. https://doi.org/10.1029/2022JA031038

Mourenas, D., Artemyev, A. V., Zhang, X. J., Angelopoulos, V., Tsai, E., & Wilkins, C. (2021). Electron lifetimes and diffusion rates inferred from ELFIN measurements at low altitude: First results. *Journal of Geophysical Research: Space Physics*, *126*, e29757. https://doi.org/10.1029/2021JA029757

Mourenas, D., Zhang, X. J., Nunn, D., Artemyev, A. V., Angelopoulos, V., Tsai, E., & Wilkins, C. (2022). Short chorus wave packets: Generation within chorus elements, statistics, and consequences on energetic electron precipitation. *Journal of Geophysical Research: Space Physics*, *127*, e30310. https://doi.org/10.1029/2022JA030310

Ni, B., Li, W., Thorne, R. M., Bortnik, J., Green, J. C., Kletzing, C. A., et al. (2014). A novel technique to construct the global distribution of whistler mode chorus wave intensity using low-altitude POES electron data. *Journal of Geophysical Research: Space Physics*, *119*, 5685–5699. https://doi.org/10.1002/2014JA019935

O'Brien, T. P., Looper, M. D., & Blake, J. B. (2004). Quantification of relativistic electron microburst losses during the GEM storms. *Geophysical Research Letters*, *31*, L04802. https://doi.org/10.1029/2003GL018621

Omura, Y., Furuya, N., & Summers, D. (2007). Relativistic turning acceleration of resonant electrons by coherent whistler mode waves in a dipole magnetic field. *Journal of Geophysical Research*, *112*, A06236. https://doi.org/10.1029/2006JA012243

Pasmanik, D. L., & Trakhtengerts, V. Y. (2005). Dispersion properties of ducted whistlers, generated by lightning discharge. *Annales Geophysicae*, *23*(4), 1433–1439. https://doi.org/10.5194/angeo-23-1433-2005

Rackauckas, C., & Nie, Q. (2017). Differentialequations.jl—A performant and feature-rich ecosystem for solving differential equations in Julia. *Journal of Open Research Software*, *5*(1), 15. https://doi.org/10.5334/jors.151

Santolík, O., Gurnett, D. A., Pickett, J. S., Parrot, M., & Cornilleau-Wehrlin, N. (2003). Spatio-temporal structure of storm-time chorus. *Journal of Geophysical Research*, *108*(A7), 1278. https://doi.org/10.1029/2002JA009791

Santolík, O., Macúšová, E., Kolmašová, I., Cornilleau-Wehrlin, N., & Conchy, Y. (2014). Propagation of lower-band whistler-mode waves in the outer Van Allen belt: Systematic analysis of 11 years of multi-component data from the Cluster spacecraft. *Geophysical Research Letters*, *41*, 2729–2737. https://doi.org/10.1002/2014GL059815

Schulz, M., & Lanzerotti, L. J. (1974). *Particle diffusion in the radiation belts*. Springer.

Sergeev, V. A., Malkov, M., & Mursula, K. (1993). Testing the isotropic boundary algorithm method to evaluate the magnetic field configuration in the tail. *Journal of Geophysical Research*, *98*(A5), 7609–7620. https://doi.org/10.1029/92JA02587

Sheeley, B. W., Moldwin, M. B., Rassoul, H. K., & Anderson, R. R. (2001). An empirical plasmasphere and trough density model: CRRES observations. *Journal of Geophysical Research*, *106*(A11), 25631–25642. https://doi.org/10.1029/2000JA000286

Shen, Y., Chen, L., Zhang, X.-J., Artemyev, A., Angelopoulos, V., Cully, C. M., et al. (2021). Conjugate observation of magnetospheric chorus propagating to the ionosphere by ducting. *Geophysical Research Letters*, *48*, e95933. https://doi.org/10.1029/2021GL095933

Shi, X., Zhang, X.-J., Artemyev, A., Angelopoulos, V., Hartinger, M. D., Tsai, E., & Wilkins, C. (2022). On the role of ULF waves in the spatial and temporal Periodicity of energetic electron precipitation. *Journal of Geophysical Research : Space Physics*, *127*, e2022JA030932. https://doi.org/10.1029/2022JA030932

Shklyar, D. R. (2021). A theory of interaction between relativistic electrons and magnetospherically reflected whistlers. *Journal of Geophysical Research: Space Physics*, *126*, e28799. https://doi.org/10.1029/2020JA028799

Shprits, Y. Y., & Ni, B. (2009). Dependence of the quasi-linear scattering rates on the wave normal distribution of chorus waves. *Journal of Geophysical Research*, *114*, 11205. https://doi.org/10.1029/2009JA014223

Shprits, Y. Y., Subbotin, D. A., Meredith, N. P., & Elkington, S. R. (2008). Review of modeling of losses and sources of relativistic electrons in the outer radiation belt II: Local acceleration and loss. *Journal of Atmospheric and Solar-Terrestrial Physics*, *70*(14), 1694–1713. https://doi.org/10.1016/j.jastp.2008.06.014

Simms, L. E., Engebretson, M. J., Clilverd, M. A., & Rodger, C. J. (2019). Ground-based observations of VLF waves as a proxy for satellite observations: Development of models including the Influence of solar Illumination and geomagnetic disturbance levels. *Journal of Geophysical Research: Space Physics*, *124*, 2682–2696. https://doi.org/10.1029/2018JA026407

Sitnov, M. I., Stephens, G. K., Tsyganenko, N. A., Miyashita, Y., Merkin, V. G., Motoba, T., et al. (2019). Signatures of nonideal plasma evolution during substorms obtained by mining multimission magnetometer data. *Journal of Geophysical Research: Space Physics*, *124*, 8427–8456. https://doi.org/10.1029/2019JA027037

Stephens, G. K., Sitnov, M. I., Korth, H., Tsyganenko, N. A., Ohtani, S., Gkioulidou, M., & Ukhorskiy, A. Y. (2019). Global empirical picture of magnetospheric substorms inferred from Multimission Magnetometer data. *Journal of Geophysical Research: Space Physics*, *124*, 1085–1110. https://doi.org/10.1029/2018JA025843

Stix, T. H. (1962). *The theory of plasma waves*. McGraw-Hill.

Streltsov, A. V., & Bengtson, M. T. (2020). Observations and modeling of whistler mode waves in the magnetospheric density ducts. *Journal of Geophysical Research: Space Physics*, *125*, e28398. https://doi.org/10.1029/2020JA028398

Summers, D., & Ni, B. (2008). Effects of latitudinal distributions of particle density and wave power on cyclotron resonant diffusion rates of radiation belt electrons. *Earth Planets and Space*, *60*(7), 763–771. https://doi.org/10.1186/bf03352825

Summers, D., Ni, B., & Meredith, N. P. (2007). Timescales for radiation belt electron acceleration and loss due to resonant wave-particle interactions: 2. Evaluation for VLF chorus, ELF hiss, and electromagnetic ion cyclotron waves. *Journal of Geophysical Research: Space Physics*, *112*, A04207. https://doi.org/10.1029/2006JA011993

Tao, X., Zonca, F., & Chen, L. (2017). Identify the nonlinear wave-particle interaction regime in rising tone chorus generation. *Geophysical Research Letters*, *44*, 3441–3446. https://doi.org/10.1002/2017GL072624

Thorne, R. M. (2010). Radiation belt dynamics: The importance of wave-particle interactions. *Geophysical Research Letters*, *372*, L22107. https://doi.org/10.1029/2010GL044990

Thorne, R. M., Li, W., Ni, B., Ma, Q., Bortnik, J., Chen, L., et al. (2013). Rapid local acceleration of relativistic radiation-belt electrons by magnetospheric chorus. *Nature*, *504*(7480), 411–414. https://doi.org/10.1038/nature12889

Thorne, R. M., O'Brien, T. P., Shprits, Y. Y., Summers, D., & Horne, R. B. (2005). Timescale for MeV electron microburst loss during geomagnetic storms. *Journal of Geophysical Research*, *110*, A09202. https://doi.org/10.1029/2004JA010882

Titova, E. E., Demekhov, A. G., Manninen, J., Pasmanik, D. L., & Larchenko, A. V. (2017). Localization of the sources of narrow-band noise VLF emissions in the range 4–10 kHz from simultaneous ground-based and Van Allen Probes satellite observations. *Geomagnetism and Aeronomy*, *57*(6), 706–718. https://doi.org/10.1134/S0016793217060135

Titova, E. E., Kozelov, B. V., Demekhov, A. G., Manninen, J., Santolik, O., Kletzing, C. A., & Reeves, G. (2015). Identification of the source of quasi-periodic VLF emissions using ground-based and Van Allen Probes satellite observations. *Geophysical Research Letters*, *42*, 6137–6145. https://doi.org/10.1002/2015GL064911

Tsai, E. (2023). Particle tracing code for energetic electrons interacting with whistler-mode waves [Software]. Zenodo. https://doi.org/10.5281/zenodo.8083874

Tsai, E., Artemyev, A., Zhang, X.-J., & Angelopoulos, V. (2022). Relativistic electron precipitation driven by nonlinear resonance with whistler-mode waves. *Journal of Geophysical Research: Space Physics*, *127*, e30338. https://doi.org/10.1029/2022JA030338

Tsurutani, B. T., & Smith, E. J. (1974). Postmidnight chorus: A substorm phenomenon. *Journal of Geophysical Research*, *79*(1), 118–127. https://doi.org/10.1029/JA079i001p00118

Tsyganenko, N. A. (1989). A magnetospheric magnetic field model with a warped tail current sheet. *Planetary and Space Science*, *37*(1), 5–20. https://doi.org/10.1016/0032-0633(89)90066-4

Tsyganenko, N. A. (1995). Modeling the Earth's magnetospheric magnetic field confined within a realistic magnetopause. *Journal of Geophysical Research*, *100*(A4), 5599–5612. https://doi.org/10.1029/94JA03193

Tsyganenko, N. A., & Sitnov, M. I. (2005). Modeling the dynamics of the inner magnetosphere during strong geomagnetic storms. *Journal of Geophysical Research*, *110*, A03208. https://doi.org/10.1029/2004JA010798

Vainchtein, D., Zhang, X. J., Artemyev, A. V., Mourenas, D., Angelopoulos, V., & Thorne, R. M. (2018). Evolution of electron distribution driven by nonlinear resonances with intense field-aligned chorus waves. *Journal of Geophysical Research: Space Physics*, *123*, 8149–8169. https://doi.org/10.1029/2018JA025654

Walsh, B. M., Hull, A. J., Agapitov, O., Mozer, F. S., & Li, H. (2020). A census of magnetospheric electrons from several ev to 30 kev. *Journal of Geophysical Research: Space Physics*, *125*, e2019JA027577. https://doi.org/10.1029/2019JA027577

Wang, D., & Shprits, Y. Y. (2019). On how high-latitude chorus waves tip the balance between acceleration and loss of relativistic electrons. *Geophysical Research Letters*, *46*, 7945–7954. https://doi.org/10.1029/2019GL082681

Wang, D., Shprits, Y. Y., Zhelavskaya, I. S., Agapitov, O. V., Drozdov, A. Y., & Aseev, N. A. (2019). Analytical chorus wave model derived from Van Allen Probe observations. *Journal of Geophysical Research: Space Physics*, *124*, 1063–1084. https://doi.org/10.1029/2018JA026183

Watt, C. E. J., Degeling, A. W., & Rankin, R. (2013). Constructing the frequency and wave normal distribution of whistler-mode wave power. *Journal of Geophysical Research: Space Physics*, *118*, 1984–1991. https://doi.org/10.1002/jgra.50231

Yearby, K. H., Balikhin, M. A., Khotyaintsev, Y. V., Walker, S. N., Krasnoselskikh, V. V., Alleyne, H. S. C. K., & Agapitov, O. (2011). Ducted propagation of chorus waves: Cluster observations. *Annales Geophysicae*, *29*(9), 1629–1634. https://doi.org/10.5194/angeo-29-1629-2011

Zhang, X. J., Agapitov, O., Artemyev, A. V., Mourenas, D., Angelopoulos, V., Kurth, W. S., et al. (2020). Phase decoherence within intense chorus wave packets constrains the efficiency of nonlinear resonant electron acceleration. *Geophysical Research Letters*, *47*, e89807. https://doi.org/10.1029/2020GL089807

Zhang, X.-J., Angelopoulos, V., Artemyev, A., Mourenas, D., Agapitov, O., Tsai, E., & Wilkins, C. (2023). Temporal scales of electron precipitation driven by whistler-mode waves. *Journal of Geophysical Research: Space Physics*, *128*, e2022JA031087. https://doi.org/10.1029/2022JA031087

Zhang, X.-J., Angelopoulos, V., Mourenas, D., Artemyev, A., Tsai, E., & Wilkins, C. (2022). Characteristics of electron microburst precipitation based on high-resolution ELFIN measurements. *Journal of Geophysical Research: Space Physics*, *127*, e30509. https://doi.org/10.1029/2022JA030509

Zhang, X.-J., Artemyev, A., Angelopoulos, V., Tsai, E., Wilkins, C., Kasahara, S., et al. (2022). Superfast precipitation of energetic electrons in the radiation belts of the Earth. *Nature Communications*, *13*(1), 1611. https://doi.org/10.1038/s41467-022-29291-8